



Hosseinalipour, S.M., Fattahi, A., Khalili, H., Tootoonchian, F. and Karimi, N. (2020) Experimental investigation of entropy waves' evolution for understanding of indirect combustion noise in gas turbine combustors. *Energy*, 195, 116978. (doi: [10.1016/j.energy.2020.116978](https://doi.org/10.1016/j.energy.2020.116978))

The material cannot be used for any other purpose without further permission of the publisher and is for private use only.

There may be differences between this version and the published version. You are advised to consult the publisher's version if you wish to cite from it.

<http://eprints.gla.ac.uk/207764/>

Deposited on 16 January 2020

Enlighten – Research publications by members of the University of  
Glasgow

<http://eprints.gla.ac.uk>

# Experimental investigation of entropy waves' evolution for understanding of indirect combustion noise in gas turbine combustors

S. M. Hosseinalipour<sup>1</sup>, A. Fattahi<sup>2,\*</sup>, H. Khalili<sup>1</sup>, F. Tootoonchian<sup>3</sup>, N. Karimi<sup>4</sup>

<sup>1</sup> School of Mechanical Engineering, Iran University of Science and Technology, Tehran, Iran

<sup>2</sup> Department of Mechanical Engineering, University of Kashan, Kashan, Iran

<sup>3</sup> Department of Electrical Engineering, Iran University of Science and Technology, Tehran, Iran

<sup>4</sup> School of Engineering, University of Glasgow, Glasgow G12 8QQ, United Kingdom

---

## Abstract

Achieving clean and quiet combustion in gas turbines is essential for improving many low-carbon energy and propulsion technologies. This often requires suppression of combustion instabilities and combustion generated noise in gas turbine combustors. Entropy noise is the less explored mechanism of combustion generated sound. Central to the emission of entropic sound is the survival of entropy wave during convection by the mean flow and reaching the combustor exit nozzle. Yet, the annihilation of entropy waves in this process is still poorly understood. To address this issue, the evolution of convected entropy waves in a fully-developed, cold flow inside a circular duct is investigated experimentally. Entropy waves are produced by a well-controlled electrical heater. Fast-response, miniaturized thermocouples arranged over a moveable cross-section of the duct are employed to record the state of entropy waves at different axial locations along the duct. Hydrodynamic parameters including Reynolds number and turbulence intensity are varied to investigate their effects upon the wave decay. The results show that the decay process is strongly wavelength dependent. It is found that the wave components with wavelengths larger than the duct diameter are almost unaffected by the flow and therefore remain essentially one-dimensional. However, other spectral components of the wave are subject to varying degrees of dissipation and loss of spatial correlation. Overall, the results support the recent numerical findings about the likelihood of wave survival in adiabatic flows. They further clarify the validity range of the one-dimensional assumption commonly made in the literature.

**Key words:** Gas turbine combustion, Entropy waves, Thermoacoustics, Indirect combustion noise, Entropy noise, Combustion instabilities.

---

## 1. Introduction

Gas turbines appear as an essential part of many low-carbon hybrid energy technologies. These include integration of gas turbines with renewable power generation [1,2] to compensate for power intermittency, combined heat and power cycles [3] for achieving high energy efficiencies and, development of solar-

assisted gas turbines for production of power, heat and freshwater [4-6]. A favorable feature of gas turbines is their fast response to load fluctuations, which distinguishes them from other power generation technologies [7]. However, generation of air pollutants, in general, and NO<sub>x</sub>, in particular, are the major concerns limiting the application of gas turbines. It is now well-demonstrated that utilization of lean premixed flames is most effective in achieving low levels of NO<sub>x</sub> emissions in power and propulsion generating gas turbines. Despite this remarkable advantage, premixed flames are quite susceptible to thermoacoustic combustion instabilities, which have emerged as the main barrier against development of lean premixed combustors [8-10]. Further, large fluctuations in load, typical of the grids partially energized by renewables, and introduction of low-carbon fuels (e.g. syngas, blends of methane and hydrogen) often intensify the susceptibility of gas turbines to combustion instabilities. These instabilities can generate high amplitude pressure waves capable of mechanically damaging the hardware and causing excessive heat transfer and thus interrupting the operation of gas turbines. Over the last few decades, significant efforts have been made to understand and suppress these instabilities [11-13]. Nonetheless, owing to their highly complex and mostly unknown physics, prediction of combustion instabilities remains as a major challenge. In general, unsteady heat release of a flame leads to oscillatory volume expansion as a source of sound. This is often regarded as direct combustion noise and, in some cases, can contribute to combustion instability [9,13,14]. Further, convection of a density inhomogeneity through a region of mean flow acceleration is another source of sound in combustors, correspondingly referred to as indirect combustion noise or entropy noise [15,16]. This terminology reflects the fact that density inhomogeneity or the so called 'entropy wave' is a gas parcel with distinctive temperature and hence entropy to those of the convecting base flow. In practice, entropy waves are generated by unsteady flames and then are carried downstream through the combustor as convective-diffusive waves. If entropy waves reach the combustor exit nozzle or the first stage of the turbine, entropy noise is emitted [17,18]. It has been shown that entropy noise may exceed direct noise and thus can be a significant source of sound in reactive systems [19]. Also, entropy noise can activate convective mechanisms of combustion instability, which are fundamentally different and less understood compared to the classical acoustic modes of thermoacoustic instability [20]. The recently growing demands for clean and quiet combustion in land-based gas turbines and aero-engines have raised a significant interest in entropy waves [21-23].

Theoretical analysis of the conversion of entropy waves into sound waves in the subcritical and supercritical nozzles was firstly conducted in the seminal work of Marble and Candel [17]. Although these authors assumed one-dimensional, linear and compact nozzle, their work continues to be a key reference after more than forty years. Recently, a number of attempts have been made to release some of the simplifying assumptions of this work. These include considering nonlinear perturbations in the compact limit [24], non-compact nozzles [25,26], piecewise-linear mean velocity profiles [27] and finite wave frequency [28].

Nonetheless, almost all existing theoretical and numerical models still assume uniform and one-dimensional entropy wave. The validity of this assumption remains unverified and therefore questionable as highlighted by Sattelmayer and co-workers [29] and further shown by the recent numerical work of Fattahi et al. [30]. This is essentially due to the dissipative effects of convecting turbulent flows, which can damage the spatial integrity of the entropy waves and thus violate the assumption of one-dimensionality. Hence, development of any predictive tool for convective thermoacoustic instabilities is subject to obtaining a thorough understanding of the spatio-temporal dynamics of entropy waves.

Due to the challenges in measuring convecting temperature fluctuations, the experimental studies of entropy waves are rather limited. The early experimental attempts on indirect noise were made by Bohn [31] and Zukoski-Auerbach [32]. They used an electrical heater that could produce an entropy wave with the amplitude of only 1K and hence their results were of limited use. More recently, Hield et al. [33] experimentally demonstrated the influences of entropy waves upon the thermoacoustic stability of a lean premixed combustor. In a separate work, these authors developed an experimental technique to measure the entropic response of the exit nozzle of a premixed combustor [34]. This was achieved by extending the classical two-microphone technique to also include a fine thermocouple [34]. The measurement technique was later improved by the same research group [35]. In a recent study, Li et al. [36] conducted energy conversion and transient growth analysis in an acoustic system, which included entropy waves convecting in non-compact nozzles. This showed that in the absence of energy exchanges between the acoustic and entropy eigenmodes, the maximum transient growth of acoustic energy would be two orders of magnitude lower than that when these eigenmodes are coupled [36]. The work of Li et al. [36] also reconfirmed that under certain conditions the entropic energy can dominate the unsteady energetics of the system [21,22].

The practical difficulties associated with the conduction of temperature measurements in combustors, have led to the development of the so called ‘Entropy Wave Generator (EWG)’. This setup produces temperature disturbances convected by a cold flow in a controlled manner. The first studies using EWG focused on the generation of entropy noise in a convergent-divergent outlet nozzle under supercritical or subcritical conditions [37,38]. A heater module produced entropy waves in a cold flow and the resultant acoustic waves in the nozzle were measured. Considering the external noise emissions, it was shown that the experiments of Bake et al. [37-39] and the analytical work of Marble and Candel [17] agreed. It was further demonstrated that the conversion of entropy waves to acoustics is dominated by Mach number, with different trends in the cold and hot flows. Although the external emission of entropy noise was investigated in detail, Refs. [37,38,40] presented no information on the dissipation of convective entropy waves. Importantly, it is noted that the temperature measurements in these studies were carried out at a single point and the spatial evolution of the wave was inevitably discarded.

In a recent experiment, aiming at reducing the core noise of a high-speed gas turbine, the entropy waves were generated by injecting hot and cold air spots at the inlet [41]. Entropy noise was then investigated in either the outlet nozzle of the combustor or at a turbine stage. Although it was stated that heat dispersion in the tubes and the mixing process downstream of the injector could affect the wave amplitude, there was no discussion on the entropy wave annihilation. In another recent study, Giusti et al. [42] developed a theoretical model, based on a novel reactive entropy wave generator, to predict the decay of entropy waves. These authors declared that Helmholtz number is the key parameter determining which annihilation mechanisms could contribute with the wave decay. **Helmholtz number is a non-dimensional frequency, defined as  $fL/c$ , in which  $f$ ,  $L$  and  $c$  are the frequency (Hz), the characteristic length and the sound speed, respectively.** Shear dispersion arising from the spatial variations of the mean velocity profile at low Helmholtz number and turbulent mixing and diffusion at high Helmholtz number were introduced as the reasons for the decay of entropy waves [42]. Similar to the previous experiments, Giusti et al. [42] made no attempt to evaluate the spatial correlation of the entropy wave.

The preceding review of the literature implies that the existing experimental studies have chiefly followed the notion of one-dimensional entropy wave and thus the spatial evolution of the wave has remained largely unexplored. However, the limited experimental [35] and numerical [30] evidence suggest that the spatial correlation of entropy wave can be influenced considerably by the hydrodynamic and thermal processes within the base flow. The resultant possibility of wave annihilation is deemed to be the reason for the current contention on the influences of entropy waves upon thermoacoustic instabilities (see [33,43,44,45]). It is expected that a convective entropy wave, being inherently a parcel of high temperature gas, is influenced by the diffusion effects of the base flow and thus may become spatially uncorrelated. Nonetheless, controversial viewpoints have arisen as the extents of the decay of entropy waves in the combustor have not been clarified yet. The recent numerical work of Fattahi et al. [30] shed some light on this problem and demonstrated that thermal non-uniformities and hydrodynamic characteristics of the flow are crucial in dissipation of entropy waves. However, that investigation was conducted on an idealized parallel-plate configuration and assumed simple thermal boundary conditions. To release these simplifying assumptions, the current work presents an experimental study of entropy waves in a cylindrical conduit with cold air flow. An electrical heater acts as an entropy wave generator and the wave evolution in the duct is detected by a set of fast-response thermocouples. These are placed across the entire cross-section of the duct to fully capture the spatio-temporal dynamics of the wave. This allows evaluating the validity of the relevant assumptions made in the literature.

## **2. Experimental methods**

### **2.1. The test rig**

The entropy wave experiment was performed in a cold duct flow. The main duct is a straight, annular tube made of clear polycarbonate with the inner diameter of 113mm. It includes the entropy wave generator and detection instruments as well as several identical sections as the main components. The working section of the rig, starting immediately downstream of the heater, has a total length of 1200mm. The long length of working section allows for examining influences of residence time on the wave decay. Fig. 1 shows a schematic view of the test rig. The flow rate of the air, supplied by a centrifugal compressor, was measured by a rotameter before entering the settling chamber. The flow was then made uniform by passing through a flow straightener, and moved through a wire net, produced by metal mesh networks, which made the turbulence intensity controllable. To prevent longitudinal variations in the flow velocity, the base flow passed through the hydrodynamic entrance length and reached the fully developed condition. To further verify this, the flow velocity profile at the test cross-section was measured at twenty-two points evenly spaced across the duct diameter by using a hotwire anemometer and the measurements were repeated at different axial locations along the duct. The turbulence intensity of the flow was also measured by the hotwire anemometer at the center of the duct. In Fig. 1 the blue directional lines present the air flow sequentially passed from the mechanical elements and the black ones are the electrical wire connected between the acquisition, control and detection instruments.

Entropy wave generator, consisting of an electrical heater module, rapidly discharges a large amount of thermal energy into the air flow. It therefore produces a temperature disturbance or a parcel of hot air with higher entropy content compared to the base flow. This parcel is then carried through the duct by the base flow and forms the entropy wave. During the experiment, the amplitude of the wave was finely controlled by the input power of the heater. The entropy wave subsequently approached the detection part equipped with fast-response thermocouples, arranged in a movable cross-section of the duct.

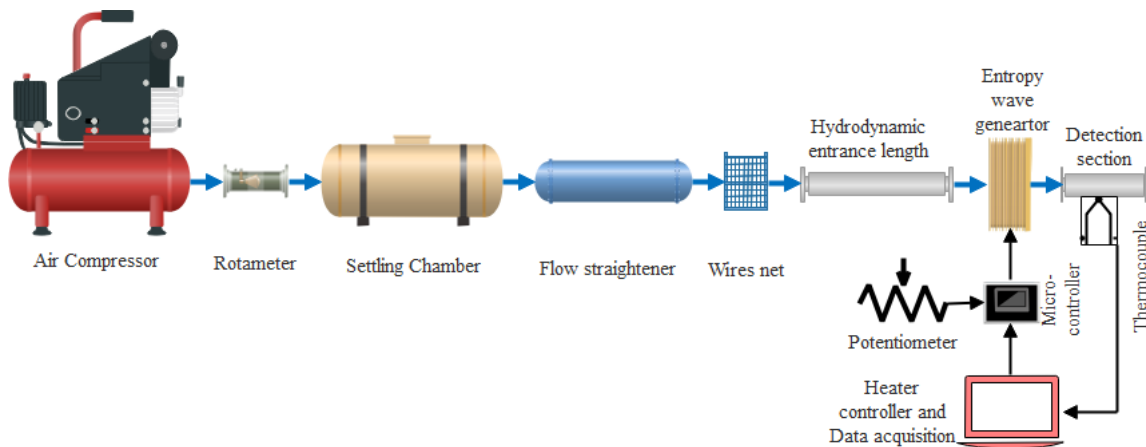


Fig. 1. Schematic view of the test rig.

## 2.2. Instrumentations

### 2.2.1. Heater module

The physics of entropy wave reveals that in the absence of acoustic perturbations, the wave reduces to a temperature disturbance ( $\frac{s'}{c_p} = \frac{T'}{T}$ ) [45,46]. This is the reason behind producing a thermal pulse as an entropy wave at the duct inlet. Entropy wave generation was performed by an electrical heater, similar to that used in the study of Bake et al. [37]. The heater is expected to discharge a large amount of thermal energy into the flow as a rapid pulse, and therefore it should have a low thermal inertia. For this purpose, it was made of thin copper wires with diameter of 100 $\mu\text{m}$ . The barrier against further reduction of the wire diameter was the concerns about the oxidation and rupture due to the passage of high electrical current. The heater consisted of five rings with wires stretched across. Each ring was joined to the neighboring one with an angle shift of  $0.4\pi$  to obtain a more uniform heat release. Fig. 2 shows a single ring and the connected rings as the heater module. Considering the desired amplitude of the entropy waves and the possibility of the copper wire oxidation, the total wire length and the distance between the parallel wires in each ring were respectively chosen to be 3.41m and 10mm. One phase from a three-phase electrical power was separated to supply a current of 50A for feeding the heater module.

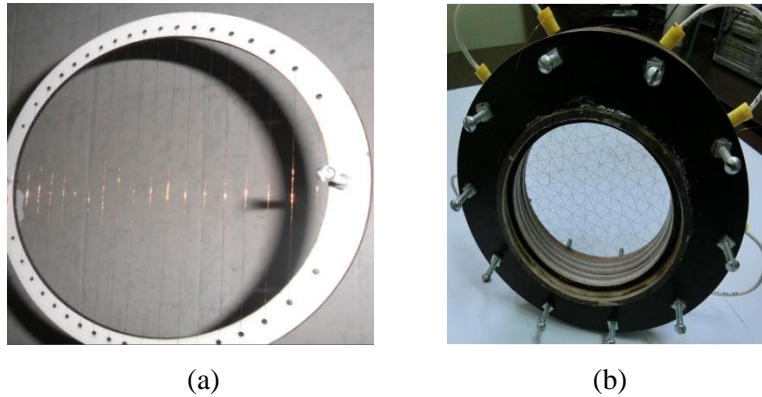


Fig. 2. (a) A single ring with the wire stretched across, (b) the heater module manufactured using five single rings.

As the heater was discharged over a fraction of a second, the electrical current consumption was measured by an oscilloscope and an electrical current sensor. Through measuring the electrical resistance of the heater, the required power was calculated. This is the amount of energy releasing into the flow field per second and reveals the entropy wave amplitude. To produce entropy waves with various amplitudes, the electrical power was changed by a 2.2Kva potentiometer with the voltage range of 75V to 102V. The controlling circuit included an optocoupler to connect the high and low voltage devices, a microcontroller and a solid-state relay.

### 2.2.2 Fast-response thermocouples

In general, measuring rapid temperature fluctuations in a flow is a confronting challenge, which requires specific developments in the conventional instruments to overcome. In this work, K-type thermocouple probes, as the most widely employed instrument in similar configurations [35,37,41], were manufactured and used. The in-house production of these probes included proper design, miniaturized manufacturing, accurate calibration and connection to downstream electronics. Assuming a miniaturized thermocouple joint without any welded bead, the lumped approach was taken to calculate the response time of the thermocouple and thus to estimate the required diameter. The thermocouple wire, as a cylinder, can be modelled as a first order linear system with time constant ( $\tau$ ) being  $\frac{\rho D c_p}{4h}$  [35]. The convective heat transfer coefficient ( $h$ ) can be then calculated by using Nusselt number correlation of Hilton [47] for the Reynolds number ranged between 4 and 40 on the basis of cylinder diameter, as the following.

$$Nu = 0.911Re^{0.385}Pr^{1/3}. \quad (1)$$

Considering the technical limitations, a minimum diameter of  $80\mu m$  was achieved, which could sense the maximum frequency of 42Hz.

TIG (Tungsten Inert Gas) welding was performed, as during the welding process of the two wires a third material should not enter the thermocouple bead. To electrically isolate the wires, they were covered by a thin lacquer layer to prevent any electrical current interference between the thermocouples situated next to each other. The manufactured micro-thermocouples were calibrated with respect to a standard thermocouple under steady and transient conditions. Nevertheless, it is noted that since in this experiment, temperature fluctuations were more important than the absolute value of temperature, a precise calibration might not be essential.

A piece of duct with the length of 200mm (and internal diameter of 113mm) equipped with 19 thermocouples was made to serve as the detection section. The thermocouples were set in three different radii (15.5mm, 31mm, 46mm) and positioned with a slight angle with respect to each other (see Fig. 3). The detection section could be desirably placed at different axial positions along the main duct of the rig through using two flange connections (see Fig. 4). To capture the data required at certain sections, this, however, was located at the inlet, middle and outlet of the main duct of the test rig.

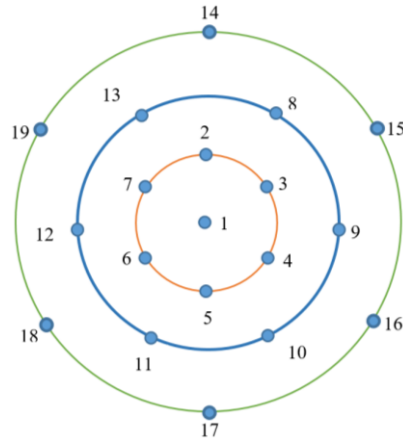
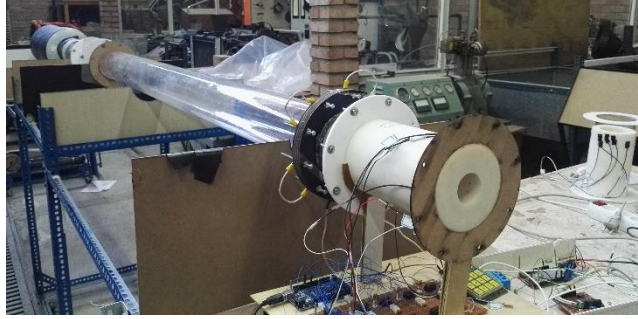


Fig. 3. Arrangement of the thermocouples inside the test cross-section. Orange and green lines show respectively the inner and outer radius (or orbit).

To amplify the weak voltage signal produced by the thermocouples, 19 IC of AD595AQ, suitable for K-type probes, were used. Two boards of Arduino MEGA2560 were hired as the data acquisition system, each one with 16 analogue channels and a microprocessor of 10 bits and the sampling frequency of 10kHz. Fig. 4a illustrates the whole detection section and data acquisition mounted on a board. The expanded uncertainty for a temperature signal extracted by each thermocouple was  $\pm 0.44^{\circ}\text{C}$ . The overall view of the test rig, with the parts earlier shown schematically in Fig. 1, is presented in Fig. 4b. The apparatus was set-up horizontally to be consistent with the most common flow direction in gas turbine combustors, which is normal to gravity. The detection section incorporated into the rig is further illustrated in Fig. 4b. This figure shows that the detection section could be replaced by any of the six identical parts of the duct and hence measurements were carried out at different axial locations along the duct.



(a)



(b)

Fig. 4. (a) The detection section and the data acquisition system prior to integration into the rig, (b) the overall view of the test rig.

### 2.3. Experimental conditions

The analyses presented in Ref. [30] revealed that turbulent flows could destroy entropy waves by subjecting them to turbulent mixing as well as hydrodynamic and thermal non-uniformities. Therefore, in the absence of steady heat transfer from the duct, entropy waves are influenced by Reynolds number ( $Re$ ) and turbulence intensity ( $TI$ ). Further, the amplitude and the width of the wave may contribute to the extent of the wave destruction [30]. In the current study, the wave amplitude and width were kept constant, respectively at the highest (288W of heater power) and lowest (0.15s for the duration of heater running) values that could be achieved by the setup, while the other parameters were varied. The duct wall could be assumed adiabatic due to low thermal conductivity of the material and high convection velocity of the wave. The experiments ran under atmospheric condition in a laboratory situated 1200m above the sea level. In the course of the experiment, the temperature of the laboratory varied between 11-13°C. Table 1 provides a list of the selected test cases. It should be emphasized that the selected Reynolds numbers are similar to those in the exiting computational studies of entropy waves [30,45].

Table 1- The investigated test cases.

Reynolds number	Turbulence intensity (%)	Case No.
13600	2	1
13600	2.8	3
6000	1.1	2
6000	1.4	4

## 3. Theoretical Methods

### 3.1. Coherence analysis

During the experiment, each thermocouple produced a temporal signal indicating the flow temperature. The evolution of entropy wave can be inferred from an analysis of the relation between the signals obtained from different points on the wave front. Spectral coherence is a statistical measure to examine how much two signals or data sets are linearly correlated. It is a real value number that falls between zero and unity; zero value means that the two signals are completely unrelated, while the unity indicates a perfect linear relation [48]. For the two signals of  $x(t)$  and  $y(t)$ , spectral coherence is defined as

$$C_{xy}(f) = \frac{G_{xy}(f)^2}{G_{xx}(f)G_{yy}(f)}, \quad (2)$$

where  $G_{xx}(f)$  and  $G_{yy}(f)$  are the auto-spectral density of  $x$  and  $y$ , respectively, and  $G_{xy}(f)$  is the cross-spectral density. These are computed with aiding the definition of mathematical expectation operator, defined as [48]

$$E[x(t)] = \int_{-\infty}^{+\infty} x(t)p(t)dt, \quad (3)$$

where  $p(t)$  is the probability density function. The expectation value for a discrete variable is the sum of the probability of each possible outcome multiplied by the outcome value [48]. The spectral densities are then calculated using Fourier transformation, denoted by the capital letters in the following expressions.

$$\begin{aligned} G_{xx}(f) &= E[X(\omega)X(\omega)], \\ G_{xy}(f) &= E[X(\omega)Y(\omega)]. \end{aligned} \quad (4)$$

The coherence function is calculated for an entropy wave between the inlet and any other cross-section along the duct. It is also conducted for two points of the wave front at a given cross-section. The coherence functions calculated for the former and the latter are presented versus Strouhal numbers, respectively indexed by 1 and 2, defined as follows.

$$\begin{aligned} St_1 &= \frac{f \cdot L}{U_b}, \\ St_2 &= \frac{f \cdot D}{U_b}, \end{aligned} \quad (5)$$

in which  $f$  is frequency (Hz),  $U_b$  is the bulk flow velocity (m/s) and  $L$  and  $D$  are the duct length and diameter (m), respectively. [This number is a non-dimensional frequency of a phenomenon related to the mean flow convection, such as entropy waves.](#)

[A major objective of the current study is evaluating the validity range of one-dimensional assumption, frequently made in entropy wave models \(see Refs. \[17,25,49\], for instance\). Such models, effectively, consider the average value of the wave over the entire duct cross-section. Thus, the average coherence is](#)

investigated here on each detection radius (or orbit) of Fig. 3 and over the entire cross-section at different axial locations. The average coherence is defined by an arithmetical average of the coherences calculated from the traces produced by Thc1 and those located on each radius, or the same thermocouple at two different axial locations. Therefore, they are given by the following relations.

$$\overline{\text{Coh}}_D = \frac{\sum_i \text{Coherence}[Thc_1(t), Thc_i(t)]}{m}, \quad (6a)$$

$$\overline{\text{Coh}}_L = \frac{\sum_j \text{Coherence}[Thc_{inlet,j}(t), Thc_{k,j}(t)]}{n}, \quad (6b)$$

in which,  $Thc_i(t)$  is the time trace obtained from the thermocouple  $i$  on either inner or outer detection radius and  $m$  is the number of thermocouples on that radius. Further, in Eq. (6b),  $j$  denotes any of the nineteen thermocouples (shown in Fig. 3) and  $k$  represents the middle or outlet test sections of the duct, while  $n$  shows the total number of thermocouples (nineteen). Subscripts  $D$  and  $L$  indicate the calculation of coherence on the cross-section or on two different axial locations. Standard deviation, as a measure of spread of the data around the mean, is used to infer the wave uniformity in the frequency domain. This is calculated by

$$SD_D^2 = \frac{[\text{Coherence}(Thc_1(t), Thc_i(t)) - \overline{\text{Coh}}_D]^2}{m}, \quad (7a)$$

$$SD_L^2 = \frac{[\text{Coherence}(Thc_{inlet,j}(t), Thc_{k,j}(t)) - \overline{\text{Coh}}_L]^2}{n}. \quad (7b)$$

$SD_D$  and  $SD_L$ , therefore, demonstrate the wave coherence variation on the transversal and longitudinal directions, respectively.

### 3.2. Wave front characterization

As the wave approaches any cross-section of the duct, the temperature starts rising at the front and then diminishes at the rear of the wave after reaching the peak value. Due to turbulent diffusion, a fraction of the thermal energy of the wave was transferred to the base flow and the air temperature subsequently rose by an infinitesimal value. This small temperature difference in the base flow before and after passage of the wave makes the wave rear unclear. In the current study, the wave rear is identified by using the following criterion,

$$\frac{T_i - T_{base}}{T_{base}} = 0.02, \quad (8)$$

where  $T_i$  is the temperature of any thermocouple on the detection cross-section and  $T_{base}$  is the temperature of the base flow in the absence of any entropy wave. The wave front is then found by setting the right-hand

side of the Eq. (8) equal to 0.001. For conciseness reasons, in the following sections “Thc” refers to thermocouple.

Time zero in the temperature capturing corresponds to the moment that the wave has been detected by the thermocouples in the test cross-section, shown in Fig. 3. Hence, the time delay due to convection of the wave from the heater to the detection cross-section has been ignored.

### 3.3. Wave dissipation and dispersion quantifying

Dissipation of an entropy wave, similar to that of a mechanical wave, can be defined as a reduction in the wave energy [50,51]. It is thus calculated by the amplitude decrement of the temperature disturbance, represented as the wave energy change. A quantitative measure of dissipation can be devised as follows.

$$\text{Dissipation } (f_a) = \frac{\mathcal{F}[(\overline{Thc}(t) |_{x_{inlet}})] - \mathcal{F}[(\overline{Thc}(t) |_{x_a})]}{\mathcal{F}[(\overline{Thc}(t) |_{x_a})]} \Big|_{f = f_a}, \quad (9)$$

where  $\mathcal{F}$  is the discrete Fourier transformation and  $\overline{Thc}(t)$  denotes the arithmetic average temperature signal, obtained from thermocouples 1 to 19. Further,  $x_a$  is the longitudinal position of an arbitrary cross-section of the duct and  $f_a$  is an arbitrary frequency. Here, the value of dissipation  $\times 100$  is regarded as dissipation index.

Convective-diffusive entropy wave may experience stretch and deformation while moving along the duct. Such deformation can vary across different frequency components of the wave and thus some of them can be cancelled out and new components may emerge. The net effect is a modification in the shape of the wave front, which can be considered as the wave dispersion. To characterize this process, a dispersion index is defined on the basis of growth or shrinkage of the wave spectral components induced by the base flow [52]. The spectral shifts of the first three maxima in the spectrum of the entropy wave form a dispersion index, defined as

$$\text{Dispersion index} = \left( \frac{\Delta f_1}{f_1} + \frac{\Delta f_2}{f_2} + \frac{\Delta f_3}{f_3} \right) \times 100, \quad (10)$$

where  $f$  denotes the frequency and digits 1 to 3 refer to the relative maxima in the wave spectrum produced by the Fourier transformation of the average thermocouple signal  $\overline{Thc}(t)$  as defined in Eq. (10). Further,  $\Delta f$  represents the spectral shift in the maximum point caused by the wave convection.

## 4. Results and Discussion

### 4.1. General behavior of the wave

As the entropy wave convects throughout the duct, it may experience dissipation and dispersion due to turbulent mixing, heat transfer and hydrodynamic non-uniformities in the flow field. In this section,

deformation and the amplitude change of the wave are examined as the indicators of the wave evolution. Precise definitions of wave dissipation and dispersion are put forward in the following sections.

Fig. 5 shows the time trace of  $\Delta T/T_{base\ flow}$  for the duration of wave convection through the duct. Here,  $\Delta T$  is the temperature rising caused by the wave and  $T_{base\ flow}$  is the base flow temperature prior to the addition of the wave. The data are presented for three different radial positions in the duct cross-section, shown in Fig.3, located at the center (Thc1) and far up (Thc14). The data were recorded for three longitudinal locations of inlet, middle and outlet. Since the heat flux releasing by the heater was constant, the wave amplitude of the high Reynolds number cases was about half of that for the low Reynolds number flows. In this figure, the dimensionless time is defined as  $time/(L/U_b)$ , in which  $L$  and  $U_b$  are the duct length and bulk flow velocity, respectively.

Figure 5 shows the typical temperature traces recorded during passage of the entropy wave. Most noticeably, the general shape of the temperature disturbance remains reasonably close to a Gaussian distribution for all locations along the duct. This is in keeping with that assumed in the numerical simulations of entropy waves [29,45]. As expected, the wave amplitude decreases during convection in the duct, indicating dissipation of the wave by the diffusion mechanisms. The extent of the amplitude loss is dependent upon the location of the thermocouple and the characteristics of the convecting flow. Figure 5 further shows that, in general, the wave width increases during the convection process. This is clearly a consequence of thermal diffusion of the initial temperature pulse into the convecting flow. However, this is not always the case as Fig. 5c shows almost no change in the wave width during the entire convection process. Although not shown here, further irregularities were observed in the traces recorded by the 19 thermocouples. These peculiarities can be attributed to the co-existence of hydrodynamic and thermal non-uniformities in the investigated flow, which makes the point-wise behavior of the wave quite involved. Such non-generalities are quite expected in a fully turbulent flow, having a wide continuum time and space scales at high Reynolds number, as the most important characteristic of the turbulence [53]. This is raised by the indeterminate and uncertain eddies interactions [53]. The non-uniformity in wave's behavior is also well-demonstrated by the recent numerical simulations of entropy wave convection [30, 54]. It will be later shown that despite these minor non-generalities, the spatially averaged characteristics of the wave front feature some regular patterns.

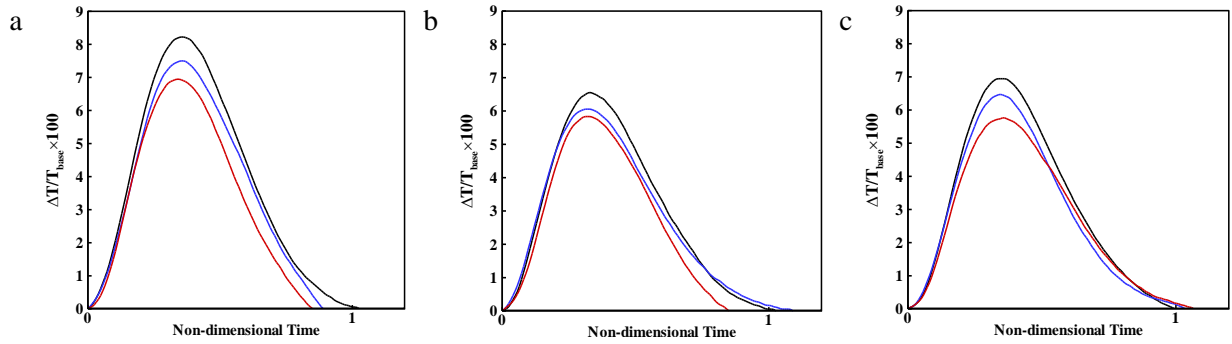


Fig. 5. Instantaneously measured  $\Delta T/T_{base\ flow}$  during convection of the entropy wave in the duct. (a) Case 1, Thc 14, (b) Case 4, Thc 14, (c) Case 4, Thc 1. Color: Black for the inlet, Blue for the middle and Red for the outlet of the duct. Dimensionless time zero refers to the moment that the wave has been detected.

#### 4.2. The wave coherence

Fig. 6 shows the coherence function calculated between the inlet and either middle or the outlet of the duct for three different thermocouples. At low frequencies (low Strouhal numbers), the coherence function takes values close to unity, reflecting a mostly undamaged wave throughout the convection process at the investigated points. This high level of correlation was also confirmed in Ref. [30], where it was shown that the waves of low frequency could largely survive the convection process.

The coherence function, however, suddenly falls at values of Strouhal number larger than 10. The coherence between the two signals takes lower values by decreasing Reynolds number and increasing turbulence intensity, as case 4 presents significant decrement in the value of coherence function in comparison with case 1. Lower values of the coherence function and scattering of that at high frequencies, for the cases with lower Reynolds number (cases 2 and 4), indicate damage to the wave integrity at the points of measurement. At low Reynolds numbers, the flow annihilating effects including hydrodynamic non-uniformities and turbulent mixing cause a significant loss of coherence. This could be explained by noting the longer (nearly twice) residence time of the wave at low Reynolds number cases compared to those with high Reynolds number. Fig. 6 implies that the waves convecting with high Reynolds number (cases 1 and 3) are more likely to maintain their coherence toward the duct outlet. Importantly, however, there appears to be strong local variations in this figure, as such the bottom thermocouple (Thc17) shows a considerably lower coherence compared to those at the center and top of the cross section (Thc1 and 14, respectively). This is

particularly visible in the low Reynolds number cases and is a confirmation of the adverse effects of the buoyancy upon the wave front.

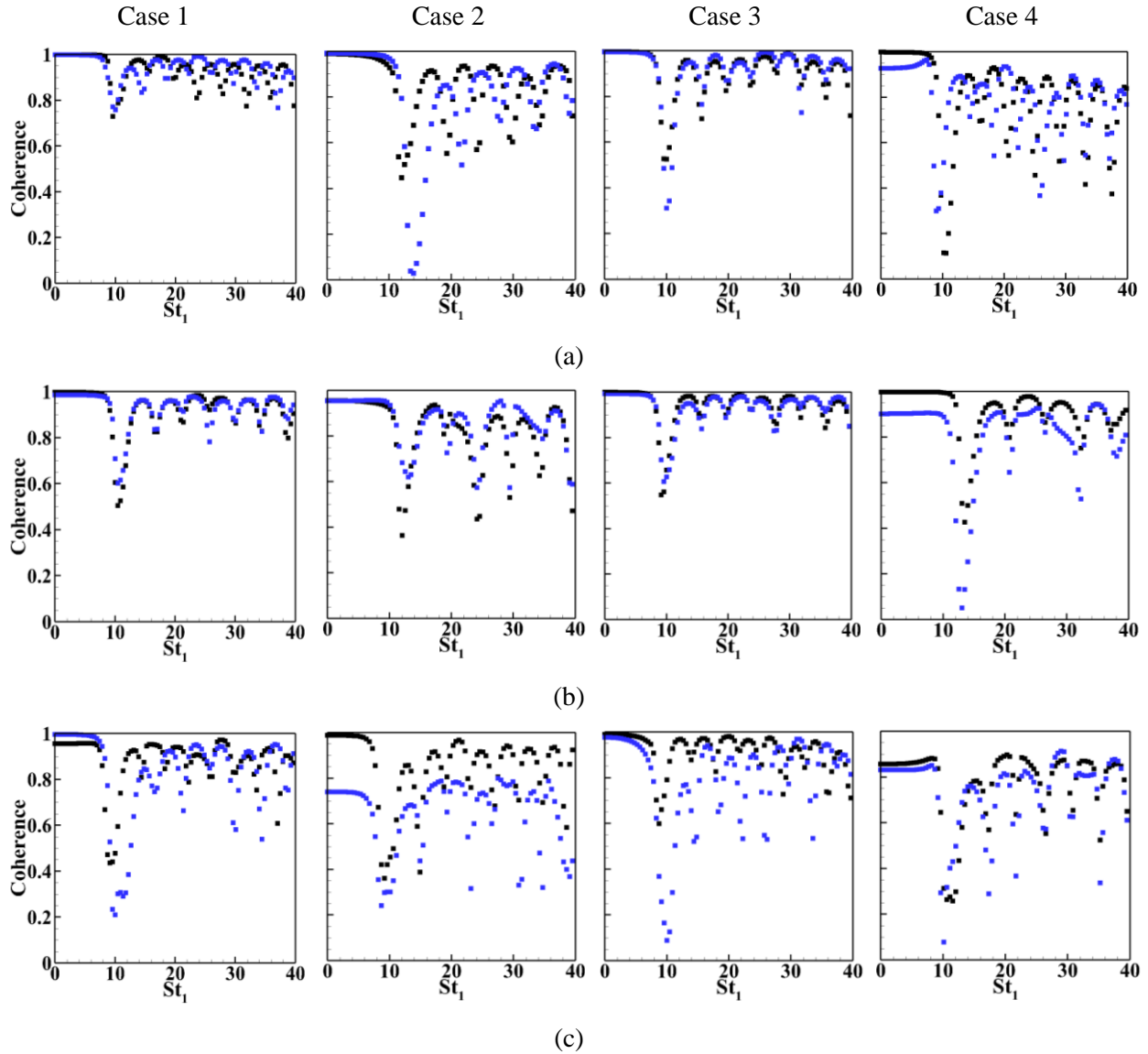


Fig. 6. Coherence functions for the temperature signals during convection of the entropy wave in the duct for (a) Thc1, (b) Thc14 and (c) Thc17. Colors: black between the inlet and middle, blue between the inlet and outlet of the duct.

The annihilating mechanisms of the flow field can destroy the spatial coherence of the wave front and ultimately break that to disjointed and diffusive pieces, which can be hardly described as a one-dimensional entropy wave. Evaluation of such destruction is of significance as it can determine the validity limits of the assumption of spatially uniform fronts. The spatial coherence of the wave front is, therefore, investigated

in Figs. 7 and 8, which present the coherence calculated between Thc1 and those located at different radii of the duct cross-section for three axial positions along the duct calculated for cases 1 and 4. It is important to recall that the length scale used in the definition of Strouhal number in Fig. 6 is different to that in Figs. 7 and 8 (see 5).

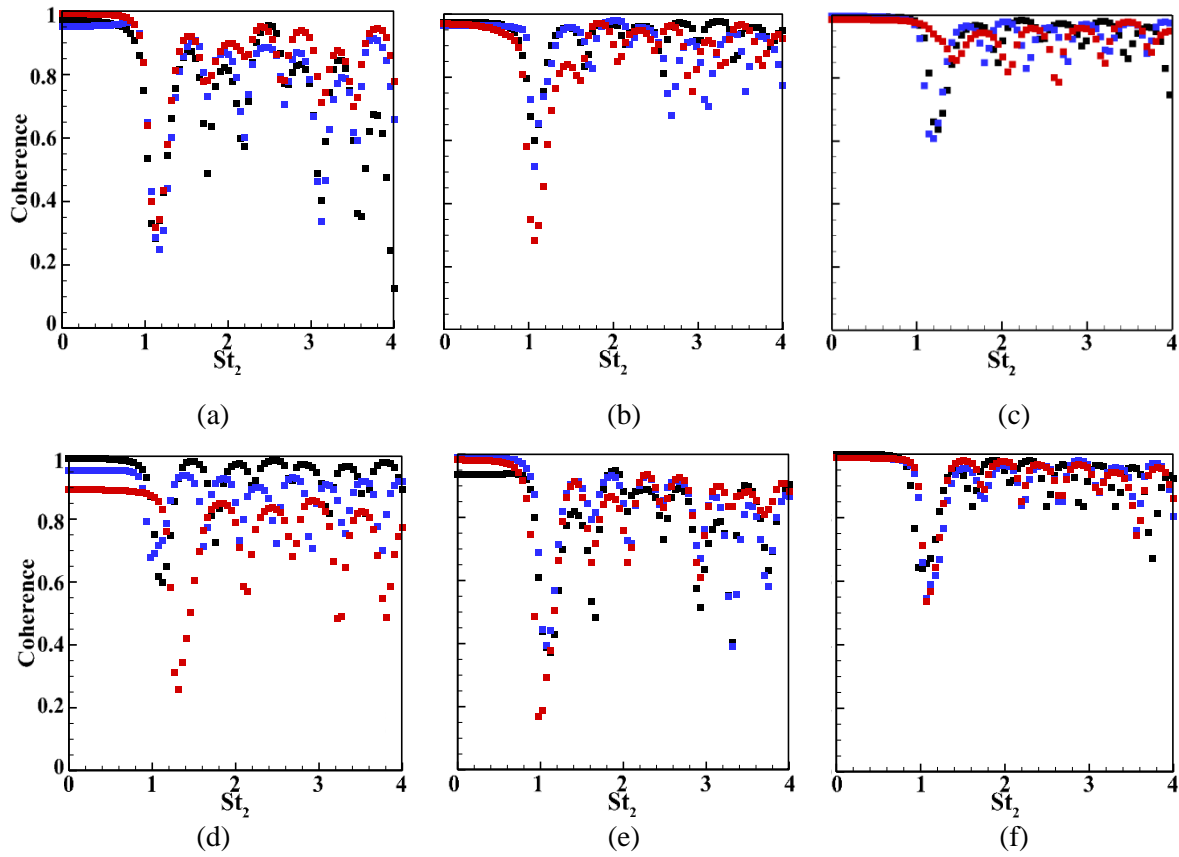
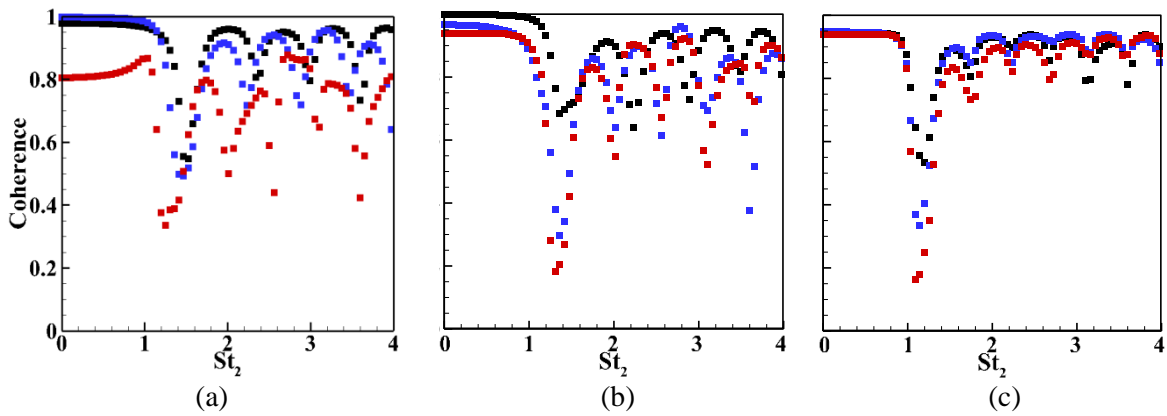


Fig. 7. Coherence function for the temperature signals of case 1 between (a) Thc1&14, (b) Thc1&13, (c) Thc 1&2, (d) Thc1&17, (e) Thc1&11, (f) Thc1&5. Colors: black for the inlet, blue for the middle and red for the outlet of the duct.



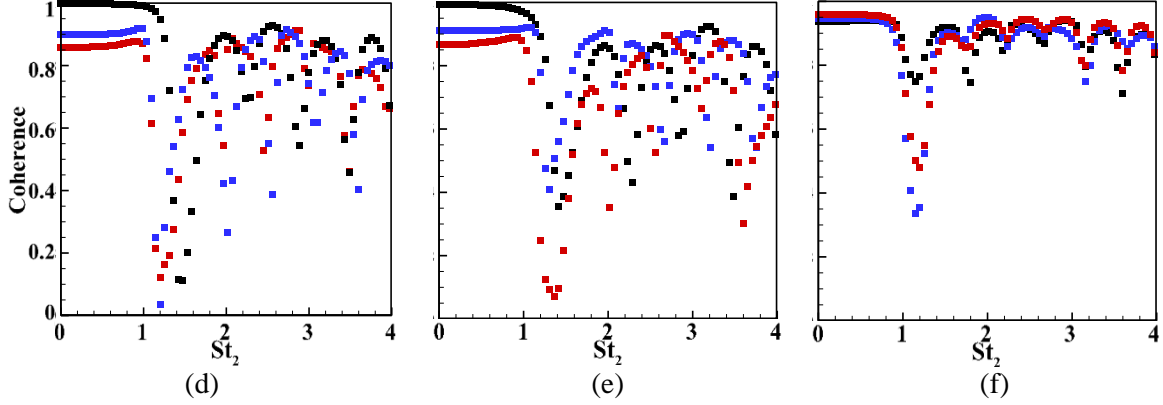


Fig. 8. Coherence function for the temperature signals of case 4 between (a) Thc1&14, (b) Thc1&13, (c) Thc1&2, (d) Thc1&17, (e) Thc1&11, (f) Thc1&5. Colors: black for inlet, blue for middle and red for outlet.

In general, Figs. 7 and 8 show that the wave remains highly correlated around the core of the duct, while coherence is poorer for the points located near the duct walls. This is to be expected, as the shear induced by the wall and the slight heat transfer between the wave and the wall tend to decay the wave. Most notably, in all investigated cases, the coherence function takes values between 0.8 and unity at low frequencies (Strouhal numbers less than one). This trend implies that low frequency (long wavelength) components of the wave may remain very well-correlated. However, high frequency components, with short time and length scales, can be readily annihilated by the turbulent flow. It is clear from Figs. 7 and 8 that the spectral distribution of coherence varies from one measurement point to another. The points on the upper half of the wave, particularly at low Reynolds number, appear more coherent than those on the lower half. As expected, the wave surface coherence takes its lowest values at the duct outlet. Increasing the turbulence intensity and decreasing Reynolds number have a deteriorating effect on the spatial coherence of the wave front, which has been further confirmed by the numerical studies [30]. Fig. 8 also shows that for the Strouhal numbers larger than one, the behavior of coherence function is heavily dependent upon the location of the measurement point. This is similar to that observed in Figs. 5 and 6 and warrants an averaging of the point-wise data.

As stated earlier at section 3.1, the value of  $SD_D$  indicates how much variation in the wave coherence occurs around a given orbit and similarly  $SD_L$  is the indicator of variations in coherence as the wave convects from the inlet to the middle and exit plan of the duct. Figs. 9 and 10 illustrate  $\overline{\text{Coh}}_D$  and  $SD_D$  for the inner and outer detection radii at the inlet and outlet (see Fig. 3 for the details). In keeping with the earlier observations, smaller changes in the coherence statistics are found in cases 1 and 3 in comparison with the

other two cases with smaller Reynolds number. These figures show that variations of  $\overline{\text{Coh}}_D$  and  $SD_D$  are more pronounced in cases 2 and 4.

Turbulent mixing in the duct flow is a main factor to annihilate the wave inside the test rig. This can more influence on the wave if the residence time, meaning total time that the wave has spent inside the test rig from the creation moment to the exit, rises. Therefore, a turbulent flow with enough residence time can make the wave spatially non-uniform. As the wave convects with the bulk flow velocity [38,39], a lower Reynolds number equals a longer residence time of the wave.

For cases with short residence time (cases 1 and 3), the average coherence is relatively higher and thus the wave is less affected by the flow. A general trend in Figs. 9 and 10 is the existence of high  $\overline{\text{Coh}}_D$  and low  $SD_D$  at low Strouhal numbers for both investigated radii and all cases. This is a strong evidence showing that, on average, low frequency waves are most likely to survive the journey throughout the duct and remain spatially correlated.

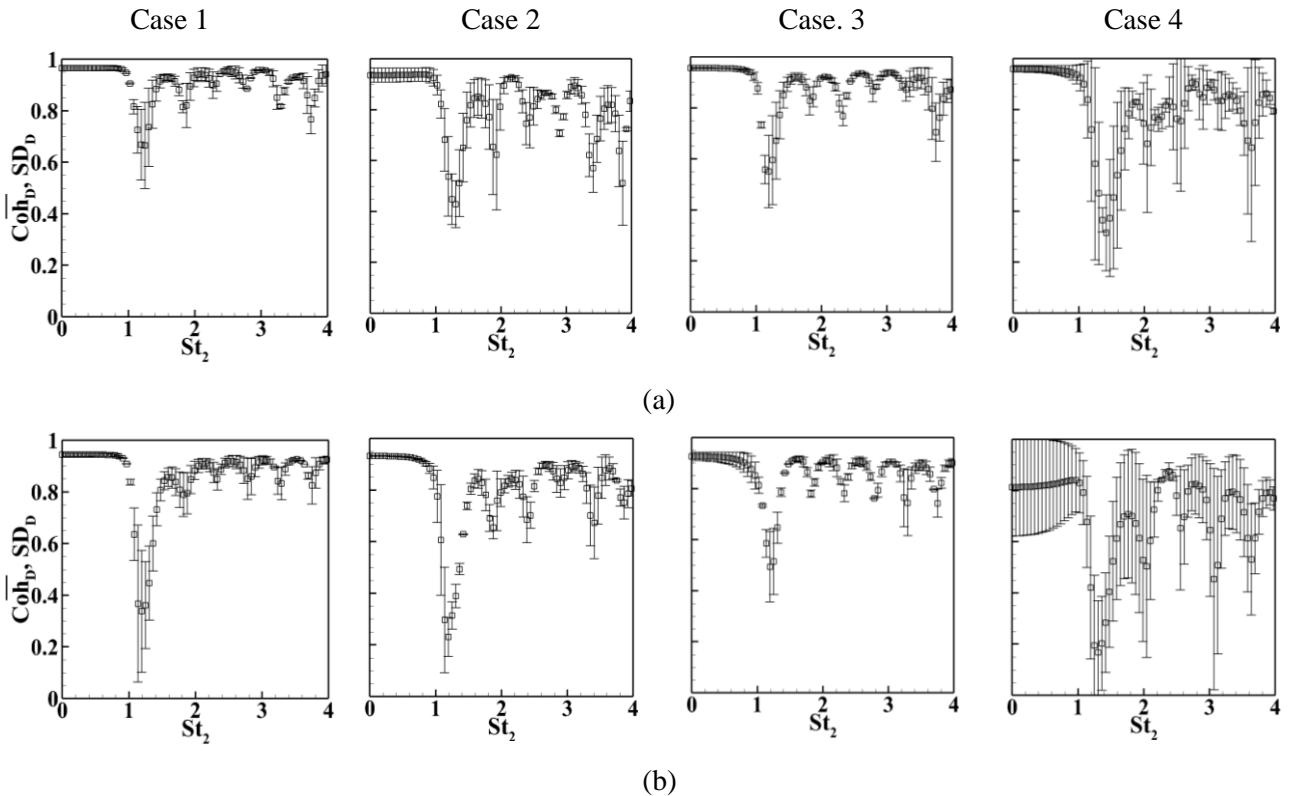


Fig. 9. Average coherence function (squares) and standard deviation (error bars) of the temperature signals obtained from Thc1 and those located on the inner orbit of the detection section, at the duct (a) inlet and (b) outlet.

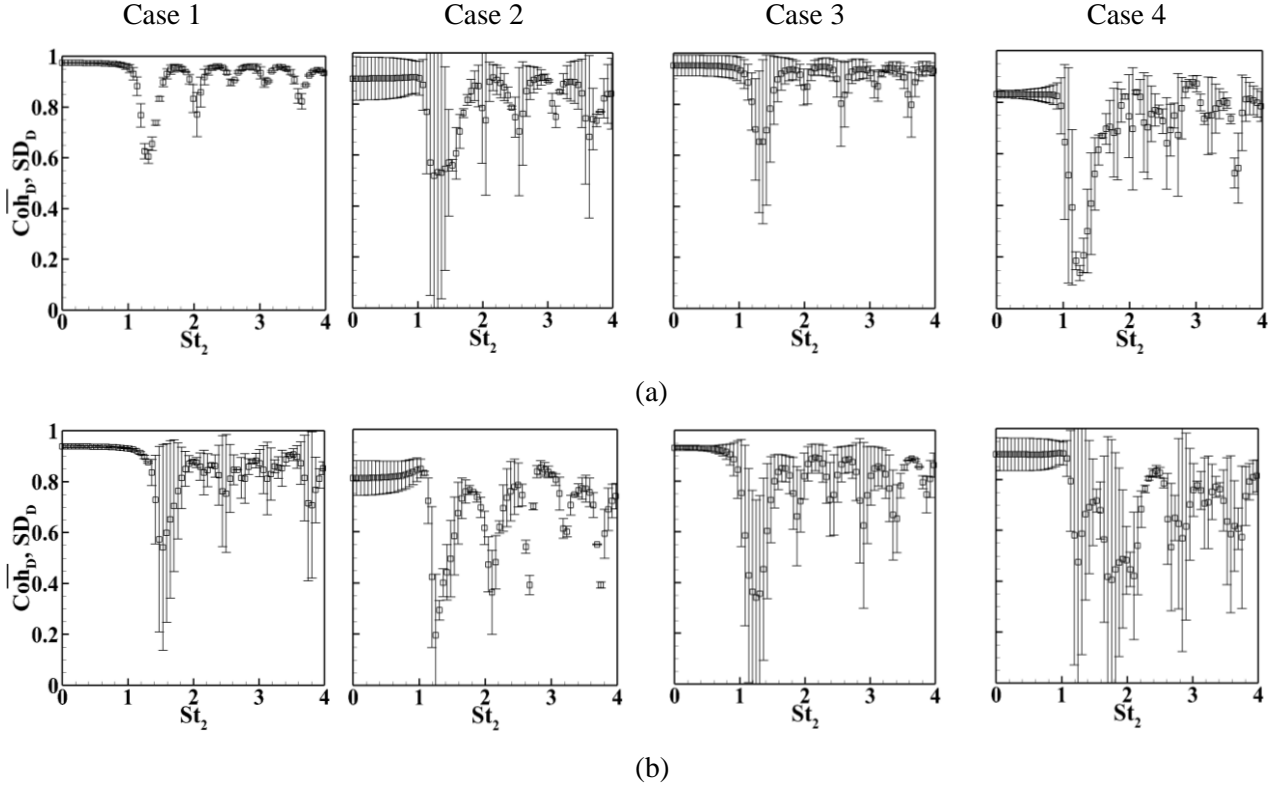


Fig. 10. Average coherence function (squares) and standard deviation (error bars) of the temperature signals obtained from Thc1 and those located on the outer orbit of the detection section, at the duct (a) inlet and (b) outlet.

The above explanation indicates that a very long duct has a major capability to affect the wave. The compact element, characterized by the so short length in comparison with the wavelength and firstly used by Marble and Candel [17], contrary, cannot remain any evolution on the wave amplitude and its temporal spectrum. Therefore, a comparison between the element's length and wavelength can somewhat clarify the extent of the wave evolution, as precisely discussed in the following.

It is essential to note that in Figs. 9 and 10 the value of  $\overline{\text{Coh}}_D$  remains close to unity up to  $St_2 \approx 1$  and then sharply declines. Given the definition of  $St_2$  in Eq. (5), this implies that on average the wave components with wavelengths larger than the duct diameter remain least affected by the flow annihilating mechanisms. This is a crucial finding as it sets a clear lower limit to the wavelengths of the entropy waves that are minimally influenced by the flow. Further, for the Strouhal numbers greater than one, the subfigures in Figs. 9 and 10 (case 1, in particular) show a series of peaks and troughs. The second trough, after the first drop of the average coherence at  $St_2 \approx 1$ , occurs at  $St_2 \approx 2$ . This is followed by a series of almost evenly

spaced troughs occurring at  $St_2 \approx 2.5, 3, 3.5$ . The Strouhal number of 2 corresponds to a wavelength matching the duct radius. Thus, those components of the entropy wave with wavelengths around the duct radius are damped more strongly. For the other observed troughs, the corresponding wavelengths are respectively  $4/5 r, 4/6 r, 4/7 r, \dots$ , where  $r$  is the duct radius, showing a series of progressively shrinking wavelengths that is attenuated by the system. Reynolds number and thus the wave residence time, which vary among the investigated cases, appear to be critical in characterizing the wave susceptibility to flow annihilating mechanisms. This can provide an explanation for the existence of contradicting conclusions in the literature on entropy waves and their pertinence to thermoacoustic stability of combustors (see for example [31,35,45,46]). Most studies that claimed a relation between entropy waves and thermoacoustic instabilities have been conducted on combustors with short residence times [35,36,55]. However, those asserting total decay of entropy waves were often concerned with the combustors featuring longer residence times [31]. Further, the observed behaviors explain the reason behind the contribution of entropy waves with combustion instability and core noise at relatively low frequencies [56,57].

As might be anticipated and also reflected by Fig. 10, at the outer measurement orbit the wave is highly affected by the flow, resulting in smaller values of  $\overline{\text{Coh}}_D$  and larger magnitude of  $SD_D$ . Further, it is inferred from Fig. 9 that even for the inner orbit of the detection section, one-dimensionality of the wave over the entire spectrum might be doubtful. Nevertheless, Figs. 9 and 10 indicate that, regardless of the flow hydrodynamics, for the frequencies corresponding to  $St_2 < 1$  the wave remains highly correlated and thus uniform. Beyond this limit, however, a truly one-dimensional entropy wave at the outlet of the duct can be realized only for high Reynolds numbers with relatively low turbulence intensity (case 1). As an essential feature, Figs. 9 and 10 show that for all investigated cases the value of  $\overline{\text{Coh}}_D$  at the duct outlet is mostly above 0.5. This implies that although entropy waves may significantly lose their spatial coherence, they are not annihilated entirely by the flow. Hence, particularly for the case at higher Reynolds number cases, some hot spots do reach the downstream nozzle. Given the relatively long duct and modest flow velocities used in this work, the current results support the arguments about the high probability of the survival of entropy waves in adiabatic duct flows [23, 45]. It is, however, essential to note that the convecting flow in real combustors can feature external heat transfer and involved aerodynamics. As already shown [30], these effects may significantly affect the spatial coherence of entropy waves.

Fig. 11 shows the average coherence,  $\overline{\text{Coh}}_L$  and standard deviation  $SD_L$  calculated for the two cross-sections located at the inlet and middle or outlet of the duct. The qualitative behavior of the average coherence and its standard deviation are similar to those discussed in Figs. 9 and 10. However, since in Fig. 11  $St_1$  (Strouhal number on the basis of the duct length) has been used, the initial highly coherent region has been

extended to  $St_1 \approx 10$ . By noting that in the test rig  $L \approx 10D$  ( $L = 1200mm, D = 113mm$ ), a similar conclusion to that obtained from Figs. 9 and 10 can be made from Fig. 11. That is the components of the entropy wave with convective wavelengths greater than the duct diameter are least influenced by the flow. In the investigated isothermal flows, wave annihilation is predominately due to turbulent diffusion. Assuming homogeneous diffusion in all directions, a wave component with the wavelength larger than the duct diameter finds a smaller chance to diffuse out compared to those components that have wavelengths shorter than the duct diameter. Hence, such long waves remain more coherent. In keeping with that observed in Figs. 9 and 10, Fig. 11 shows that as the wave convects through the duct, the average value of the coherence drops, and the magnitude of standard deviation increases, while the average coherence is mostly above 0.5.

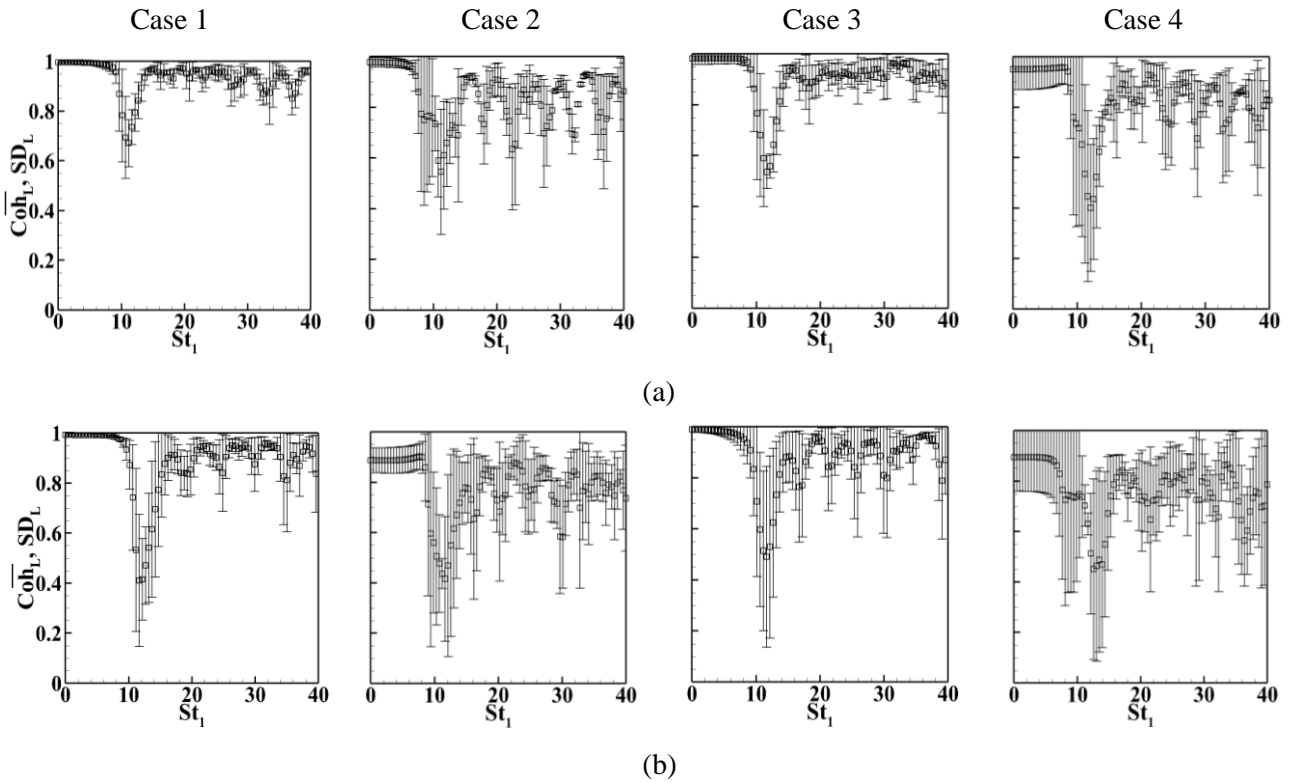


Fig. 11. Average coherence function (squares) and standard deviation (error bars) of the temperature signals obtained by each thermocouple between (a) inlet and middle and (b) inlet and outlet of the duct.

### 4.3. Wave dissipation and dispersion

Fig. 12 depicts the values of dissipation index calculated over a frequency range and at different cross-sections along the duct. In keeping with the earlier results, dissipation index appears to be negligible at low frequencies (long convective wavelength). As the Strouhal number increases, dissipation index takes higher values and rises by increasing turbulence intensity or decreasing Reynolds number. Further, it becomes

larger as the distance between the investigated cross-section and the duct inlet increases, which is a consequence of the longer time given to the flow annihilating mechanisms to dissipate the wave. Fig. 12 shows that, at high frequencies and depending upon the flow hydrodynamics, the ratio of the dissipation indices evaluated at the duct outlet and inlet can reach up to three. However, regardless of the values of Reynolds number and turbulence intensity, the ratio of these two is always close to unity at low frequencies. Once again, this implies that low frequency components of the wave are largely unaffected by the flow.

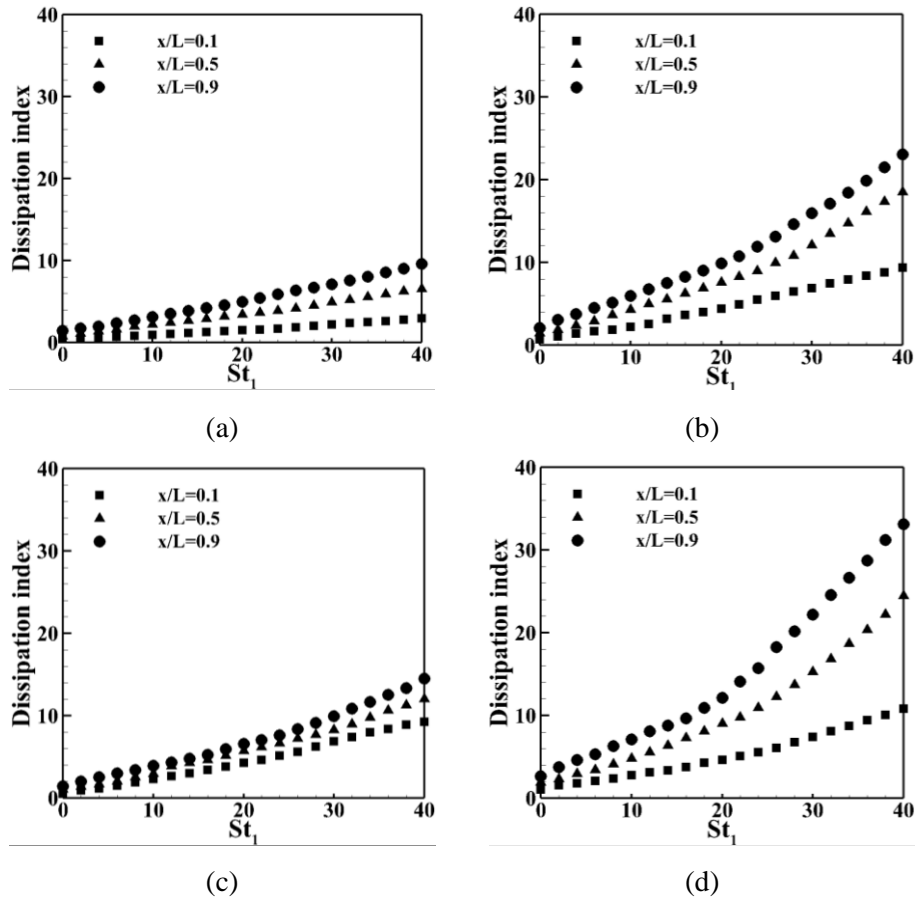


Fig. 12. Dissipation indices (defined by Eq. 9) versus Strouhal number for (a) case 1, (b) case 2, (c) case 3, (d) case 4.

Further, the difference between the values of dissipation index evaluated at the first and second cross-sections (at  $\frac{x}{L} = 0.1$  &  $0.5$ ) are larger than that between the second and third cross-sections (at  $\frac{x}{L} = 0.9$ ). This clearly shows that the wave dissipation strongly depends on the thermal energy of the wave as a major part of such energy is lost during the early stages of wave convection, where the amplitude is still large and thus there is a higher potential for heat diffusion in to the base flow.

Fig. 13 shows that in general the dispersion index grows by approaching the duct outlet, while the extent of this growth is different among the four investigated cases. Close to the duct outlet, the lowest value of dispersion index (~15%) belongs to case 1 with high Reynolds number and relatively high turbulence intensity. Reducing the Reynolds number and turbulence intensity by almost a factor of two, in case 2, result in a significant increase in wave dispersion at the same cross-section. However, a large increase of these parameters in case 3 increases the dispersion index slightly. The highest value of dispersion index at  $\frac{x}{L} = 0.9$  corresponds to case 4 with low Reynolds number and a rather small turbulence intensity. Making a definitive conclusion about the relative significance of Reynolds number and turbulence intensity in quantifying the dispersion index is difficult. Nonetheless, the presented data imply that Reynolds number can have a pronounced effect upon the dispersion of entropy wave. The qualitative trend in the wave dispersion agrees with those discussed earlier regarding dissipation index. Further, the differences in the dispersion indices of various cases appear to be negligible near the duct inlet. Yet, they rise significantly as the wave convects along the duct and dispersion index can exceed 45% at the duct outlet, indicating a major reshaping of the initial wave front. These show that the state of entropy wave can be largely altered by the base flow and that the front can be highly dispersed. Such dispersion is a sign of considerable annihilation of the entropy wave and in case of partial survival of the wave, it can considerably influence the generated entropy noise [58].

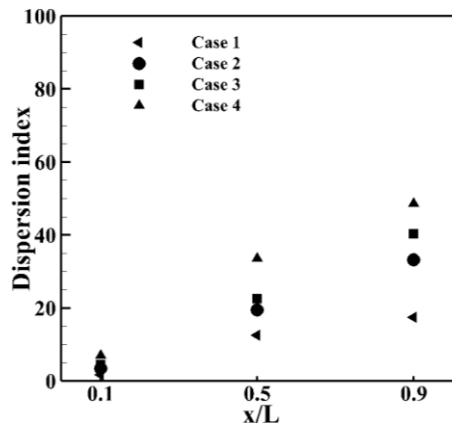


Fig. 13. Entropy wave dispersion.

## 5. Conclusions

Indirect combustion noise is the less explored mechanism of sound generation in combustors that can lead to noise emission and combustion instability. Understanding and suppression of this mechanism is key to the development of clean energy technologies that involve gas turbines. Spatio-temporal evolution of

convective entropy waves was investigated experimentally in a cold, turbulent flow inside a cylindrical conduit. The entropy wave was generated by an electrical heater module. Evaluations of the wave, as a convective heat pulse, was carried out by using nineteen fast-response, miniaturized K-type thermocouples, arranged over a movable cross-section of the duct. Coherence functions and their statistics were used to post-process the recorded data, while two indices were introduced to measure the decay and dispersion of the wave. The presented work is the first experimental analysis of the spatial correlation of entropy waves. The main findings of this study are as follows.

In keeping with other recent investigations, it was found that the wave dissipation and dispersion were strongly affected by the characteristics of the convecting flow. In particular, long residence times and high turbulence intensities tend to dissipate and disperse the entropy wave. Importantly, the low frequency components of the wave with convective wavelengths larger than the duct diameter remain highly coherent throughout the duct. This was evidenced by close to unity values of the average coherence function with small magnitude of standard deviation for Strouhal numbers less than unity, indicating little annihilation of these low-frequency components during the convection process. Shorter wavelengths (higher Strouhal numbers) experience varying levels of destruction, which can render the wave spatially uncorrelated. Nonetheless, in agreement with the recent numerical studies it was observed that for all investigated cases, some hot spots could reach the duct outlet. It was further shown that for cold duct flows, the one-dimensional description of entropy wave is strictly correct for the Strouhal numbers less than unity (based on duct diameter) or short ducts. Beyond these conditions, validity of the one-dimensional assumption is considerably influenced by the hydrodynamics of the flow under investigation. More specifically, the entropy waves experiencing large Reynolds numbers and low turbulence intensities are likely to remain highly spatially coherent and hence can be approximated as one-dimensional waves.

It is crucial to recall that the conclusions made here are restricted to the investigated nearly-adiabatic flows. Major heat losses from the base flow and more complicated flow configurations can significantly intensify the wave decay and therefore lead to total annihilation of entropy waves.

### **Acknowledgement**

Nader Karimi acknowledges the partial support of EPSRC through grant number EP/N020472/1.

### **References**

- [1] G. Guandalini, S. Campanari, M. C. Romano, "Power-to-gas plants and gas turbines for improved wind energy dispatchability: Energy and economic assessment," *Appl. Energ.* 147, 117, 2015.

- [2] J. Kotowicz, M. Brzęczek, M. Job, "The thermodynamic and economic characteristics of the modern combined cycle power plant with gas turbine steam cooling," *Energy*, 164, 359 (2018).
- [3] M. Ni, T. Yang, G. Xiao, D. Ni, X. Zhou, H. Liu, U. Sultan, J. Chen, Z. Luo, K. Cen, "Thermodynamic analysis of a gas turbine cycle combined with fuel reforming for solar thermal power generation." *Energy*, 20, 137 (2017).
- [4] G. J. Nathan, M. Jafarian, B. B. Dally, W. L. Saw, P. J. Ashman, E. Hu, A. Steinfeld, "Solar thermal hybrids for combustion power plant: A growing opportunity," *Prog. Energy Combust. Sci.* 64, 4 (2018).
- [5] Y.N. Dabwan, P. Gang, J. Li, G. Gao, J. Feng, "Development and assessment of integrating parabolic trough collectors with gas turbine trigeneration system for producing electricity, chilled water, and freshwater," *Energy*, 162, 364 (2018).
- [6] A. Di Gaeta, F. Reale, F. Chiariello, P. Massoli, "A dynamic model of a 100 kW micro gas turbine fuelled with natural gas and hydrogen blends and its application in a hybrid energy grid," *Energy*, 129, 299 (2017).
- [7] T.S. Pires, M.E. Cruz, M.J. Colaço, M.A. Alves, "Application of nonlinear multivariable model predictive control to transient operation of a gas turbine and NOX emissions reduction," *Energy*, 149, 341 (2018).
- [8] T. C. Lieuwen, "Unsteady combustor physics," Cambridge University Press, (2012).
- [9] W. C. Strahle, "On combustion generated noise," *J. Fluid Mech.* **49**(2), 399 (1971).
- [10] N. Karimi, "Response of a conical, laminar premixed flame to low amplitude acoustic forcing—A comparison between experiment and kinematic theories," *Energy*, 78, 490 (2014).
- [11] S. Candel, "Combustion dynamics and control: Progress and challenges," *Proc. Combust. Inst.* **29**(1), 1 (2002).
- [12] T. Poinso, "Prediction and control of combustion instabilities in real engines," *Proc. Combust. Inst.* **36**, 1 (2016).
- [13] S. Candel, D. Durox, T. Schuller, N. Darabiha, L. Hakim, T. Schmitt, "Advances in combustion and propulsion applications," *Eur J Mech B Fluids* **40**, 87 (2013).
- [14] S. Candel, D. Durox, S. Ducriux, A.-L. Birbaud, N. Noiray, T. Schuller, "Flame dynamics and combustion noise: progress and challenges," *Int. J. Aeroacoustics* **8**(1), 1 (2009).
- [15] M. Howe, "Contributions to the theory of aerodynamic sound, with application to excess jet noise and the theory of the flute," *J. Fluid Mech.* **71**, 625 (1975).
- [16] J. E. Ffwoocs Williams and M. Howe, "The generation of sound by density inhomogeneities in low Mach number nozzle flows," *J. Fluid Mech.* **70**, 605 (1975).

- [17]F. E. Marble and S. M. Candel, "Acoustic disturbance from gas non-uniformities convected through a nozzle," *J. Sound Vib.* **55**(2), 225 (1977).
- [18]N. A. Cumpsty and F. E. Marble, "Core noise from gas turbine exhausts," *J. Sound Vib.* **54**(2), 297 (1977).
- [19]M. Leyko, F., Nicoud, T., Poinot, "Comparison of direct and indirect combustion noise mechanisms in a model combustor," *AIAA J.* 47(11), 2709 (2009).
- [20]A. S. Morgans and I. Duran, "Entropy noise: A review of theory, progress and challenges," *Int. J. Spray Combust. Dyn.* **8**(4), 285 (2016).
- [21]N. Karimi, M. J., Brear, W. H. Moase, "Acoustic and disturbance energy analysis of a flow with heat communication," *J. Fluid Mech.* **597**, 67 (2008).
- [22]N. Karimi, M. Brear, and W. Moase, "On the interaction of sound with steady heat communicating flows," *J. Sound Vib.* **329**(22), 4705 (2010).
- [23]C. S. Goh, A. S. Morgans, "The influence of entropy waves on the thermoacoustic stability of a model combustor," *Comb. Sci. Tech.* **185**(2), 249 (2013).
- [24]M. Huet and A. Giauque, "A nonlinear model for indirect combustion noise through a compact nozzle," *J. Fluid Mech.* **733**, 268 (2014).
- [25]C. S. Goh and A. S. Morgans, "Phase prediction of the response of choked nozzles to entropy and acoustic disturbances," *J. Sound Vib.* **330**, 5184 (2011).
- [26]S.M. Hosseinalipour, A. Fattahi, N. Karimi, "Investigation of the transmitted noise of a combustor exit nozzle caused by burned hydrogen-hydrocarbon gases," *Int. J. Hydrogen Energy* **41**, 2075 (2016).
- [27]A. Giauque, M. Huet, F. Clero, "Analytical analysis of indirect combustion noise in subcritical nozzles," *J Eng. Gas Turbine Power* **134**(11), 111202 (2012).
- [28]S. R. Stow, A. P. Dowling, T. P. Hynes, "Reflection of circumferential modes in a choked nozzle," *J. Fluid Mech.* **467**, 215 (2002).
- [29]T. Sattelmayer, "Influence of the combustor aerodynamics on combustion instabilities from equivalence ratio fluctuations," *J. Eng. Gas Turbines Power* **125**, 11 (2003).
- [30]A. Fattahi, S. M. Hosseinalipour, N. Karimi, "On the dissipation and dispersion of entropy waves in heat transferring channel flows," *Phys. Fluids*, **29**(8), 087104 (2017).
- [31]M. S. Bohn, "Noise produced by the interaction of acoustic waves and entropy waves with high-speed nozzle flows," California Institute of Technology, (1976).
- [32]E. E. Zukoski, J. M. Auerbach, "Experiments concerning the response of supersonic nozzles to fluctuating inlet conditions," *J. Eng. Gas Turbine Power*, **98**(1), 60 (1976).

- [33]P. A. Hield, M. J. Brear, and S. H. Jin, "Thermoacoustic limit cycles in a premixed laboratory combustor with open and choked exits," *Combust. Flame* **156**, 1683 (2009).
- [34]P. A. Hield and M. J. Brear, "Comparison of open and choked premixed combustor exits during thermoacoustic limit cycle," *AIAA J.* **46**(2), 517 (2008).
- [35]D. Carolan, "Measurement of the Transfer Function of a Combustor Exit Nozzle," MSc dissertation, University of Melbourne, Department of Mechanical Engineering, (2009).
- [36]L. Li, D. Zhao, X. Yang, "Effect of entropy waves on transient energy growth of flow disturbances in triggering thermoacoustic instability," *Int. J. Heat Mass Transfer* **99**, 219 (2016).
- [37]F. Bake, U. Michel, I. Roehle, "Investigation of entropy noise in aero-engine combustors," *J. Eng. Gas Turbine Power* **129**(2), 370 (2007).
- [38]F. Bake, N. Kings, and I. Roehle, "Fundamental mechanism of entropy noise in aero-engines: Experimental investigation," *J. Eng. Gas Turbines Power* **130**(1), 011202 (2008).
- [39]F. Bake, C. Richter, B. Muhlbauer, N. Kings, I. Rohle, F. Thiele, and B. Noll, "The entropy wave generator (EWG): a reference case on entropy noise," *J. Sound Vib.* **326**(3), 574 (2009).
- [40]A. Rausch, A. Fischer, H. Konle, A. Gaertlein, S. Nitsch, K. Knobloch, F. Bake, I. Röhle, "Measurements of density pulsations in the outlet nozzle of a combustion chamber by Rayleigh-scattering searching entropy waves," *J. Eng. Gas Turbine Power* **133**(3), 031601 (2011).
- [41]G. Persico, P. Gaetani, A. Spinelli, "Assessment of synthetic entropy waves for indirect combustion noise experiments in gas turbines," *Exp. Therm. Fluid Sci.* **88**, 376 (2017).
- [42]A. Giusti, N. A. Worth, E. Mastorakos, A. P. Dowling, "Experimental and numerical investigation into the propagation of entropy waves," *AIAA J.*, **55**(2), 446 (2016).
- [43]J. Eckstein, E. Freitag, C. Hirsch, T. Sattelmayer, "Experimental study on the role of entropy waves in low-frequency oscillations in a RQL combustor," *J. Eng. Gas Turbine Power* **128**(2), 264 (2006).
- [44]J. Eckstein and T. Sattelmayer, "Low-order modeling of low-frequency combustion instabilities in aeroengines," *J. Propul. Power* **22**, 425 (2006).
- [45]A. S. Morgans, C. S. Goh, and J. A. Dahan, "The dissipation and shear dispersion of entropy waves in combustor thermoacoustics," *J. Fluid Mech.* **733**, R2 (2013).
- [46]A.P. Dowling, S. R. Stow. "Acoustic analysis of gas turbine combustors." *J. Propul Power* **19.5**, 751 (2003).
- [47]T. L. Bergman, F. P. Incropera, A. S. Lavine, D. P. Dewitt, "Introduction to heat transfer," John Wiley & Sons, (2011).
- [48]D. C. Montgomery, G. C. Runger, "Applied statistics and probability for engineers," John Wiley & Sons, (2010).

- [49] W. H. Moase, M. J. Brear, and C. Manzie, "The forced response of choked nozzles and supersonic diffusers," *J. Fluid Mech.* **585**, 281 (2007).
- [50] M. Hosseinalipour, A. Fattahi, A. Afshari, and N. Karimi, "On the effects of convecting entropy waves on the combustor hydrodynamics," *Appl. Therm. Eng.* **110**, 901 (2017).
- [51] J. Lighthill, M. J. Lighthill, "Waves in fluids," Cambridge university press, (2001).
- [52] G. Whitham, "Linear and nonlinear waves," John Wiley & Sons, (1974).
- [53] Mathieu, J., & Scott, J. (2000). *An introduction to turbulent flow*. Cambridge University Press.
- [54] W. H. Moase, M. J. Brear, and C. Manzie, "The forced response of choked nozzles and supersonic diffusers," *J. Fluid Mech.* **585**, 281 (2007).
- [55] E. Motheau, F. Nicoud, T. Poinsot, "Mixed acoustic-entropy combustion instabilities in gas turbines," *J. Fluid Mech.* **749**, 542 (2014).
- [56] D. Wassmer, B. Schuermans, C. O. Paschereit and J. P. Moeck, "An acoustic time-of-flight approach for unsteady temperature measurements: Characterization of entropy waves in a model gas turbine combustor," *J. Eng. Gas Turbine Power*, **139**(4), 041501(2017).
- [57] D. Wassmer, B. Schuermans, C. O. Paschereit and J. P. Moeck, "Measurement and modeling of the generation and the transport of entropy waves in a model gas turbine combustor," *Int. J. Spray Combust. Dyn.* **9**(4), 299-309 (2017).
- J. M. Lourier, A. Huber, B. Noll, M. Aigner, "Numerical analysis of indirect combustion noise generation within a subsonic nozzle". *AIAA J.* **52**(10), 2114 (2014).